DOI: 10.1002/chem.201001572

Site-Directed Spin-Labeling of DNA by the Azide–Alkyne 'Click' Reaction: Nanometer Distance Measurements on 7-Deaza-2′-deoxyadenosine and 2′-Deoxyuridine Nitroxide Conjugates Spatially Separated or Linked to a 'dA-dT' Base Pair

Ping Ding,[a, b] Dorith Wunnicke,[c] Heinz-Jürgen Steinhoff,*[c] and Frank Seela*[a, b]

Abstract: Nucleobase-directed spin-labeling by the azide-alkyne 'click' (CuAAC) reaction has been performed for the first time with oligonucleotides. 7-Deaza-7-ethynyl-2′-deoxyadenosine (**1**) and 5-ethynyl-2′-deoxyuridine (**2**) were chosen to incorporate terminal triple bonds into DNA. Oligonucleotides containing **1** or **2** were synthesized on a solid phase and spin labeling with 4-azido-2,2,6,6-tetramethylpiperidine 1-oxyl (4-azido-TEMPO, **3**) was performed by post-modification in solution. Two spin labels (**3**) were incorporated with high efficiency into the DNA duplex at spatially separated positions or into a 'dA-dT' base pair. Modification at the 5-position of the pyrimidine base or at the 7-position of the 7-deazapurine residue gave steric freedom to the spin label in the major groove of duplex DNA. By applying cw and pulse EPR spectroscopy, very accurate distances between spin labels, within the range of 1–2 nm, were measured. The spin–spin distance was 1.8 ± 0.2 nm for DNA duplex **17**(**dA***^{7,10})·**11** containing two spin labels that are separated by two nucleotides within one individual strand. A distance of 1.4 ± 0.2 nm was found for the spin-labeled 'dA-dT' base pair **15**(**dA***^{7})·**16**(**dT***^{6}). The 'click' approach has the potential to be applied to all four constituents of DNA, which indicates the universal applicability of the method. New insights into the structural changes of canonical or modified DNA are expected to provide additional information on novel DNA structures, protein interaction, DNA architecture, and synthetic biology.

Keywords: click chemistry · DEER spectroscopy · EPR spectroscopy · oligonucleotides · spin labeling

Introduction

DNA is a polymorphic molecule that forms a variety of three-dimensional structures such as A-, B-, or Z-DNA as well as other motifs. Different base sequences can influence structural parameters such as groove width, local twist, curvature, and mechanical rigidity.[1] These features help proteins to read and recognize one oligonucleotide sequence in preference to another, not only through the chemical properties in the positions of nucleotide residues, but also through sequence-dependent structural features.[2]

During the last decade electron paramagnetic resonance (EPR) spectroscopy in combination with site-directed spin labeling (SDSL) has emerged as a powerful tool for investigating RNA/DNA architectures under biological conditions.[3] Recently, pulse EPR spectroscopy has been applied to DNA, focusing on B/A conformational transitions[4] and DNA damage,[5] and a nanometer distance ruler based on folded DNA/RNA has been developed.[6] To apply EPR spectroscopic protocols to DNA, unpaired electron spins

[a] P. Ding, Prof. F. Seela
Laboratory of Bioorganic Chemistry and Chemical Biology
Center for Nanotechnology
Heisenbergstrasse 11, 48149 Münster (Germany)
Fax: (+49) 251-53406857
E-mail: frank.seela@uni-osnabrueck.de
seela@uni-muenster.de

[b] P. Ding, Prof. F. Seela
Laboratorium für Organische und Bioorganische Chemie
Institut für Chemie, Universität Osnabrück
Barbarastrasse 7, 49069 Osnabrück (Germany)
Fax: (+49) 251-53406857

[c] D. Wunnicke, Prof. H.-J. Steinhoff
Fachbereich Physik, Universität Osnabrück
Barbarastrasse 7, 49069 Osnabrück (Germany)
Fax: (+49) 541-969-2656
E-mail: hsteinho@uni-osnabrueck.de

Supporting information for this article is available on the WWW under http://dx.doi.org/10.1002/chem.201001572.

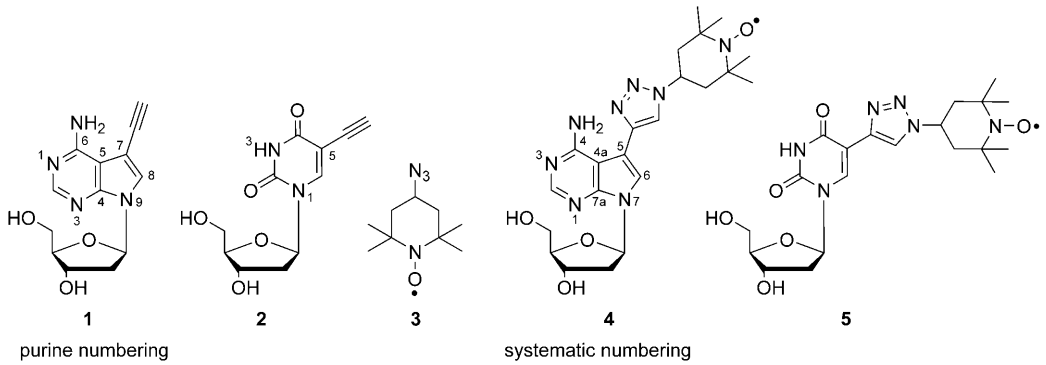

Figure 1. Structures of the ethynyl-substituted nucleosides and 4-azido-TEMPO conjugates.

have to be introduced and several paramagnetic species can be chosen for this purpose, for example, metal ions, Cu^{2+} or FeS clusters, radical centers, and nitroxide spin labels that are chemically stable and geometrically fairly rigid.[3] Incorporation of spin labels into oligonucleotides should occur at defined positions with high efficiency causing only small structural perturbations of the DNA structure. However, the spin label should be rigid enough to reduce motion that obscures physical data.

Continuous wave (cw) EPR analysis of spin-labeled biomolecules provides information about the mobility of the nitroxide side chain,[3] the polarity of its microenvironment,[7] and the intra- or intermolecular distances between two spin-labeled side chains in the distance range of 1–2 nm.[8] Double electron electron resonance (DEER) spectroscopy extends the measurable interspin distances to up to 8 nm.[9] Several approaches have been applied to the spin labeling of RNA/DNA, as recently reviewed by Klare and Steinhoff.[10] The nitroxide side-chains can be introduced on the monomeric level, into phosphoramidites for solid-phase oligonucleotide synthesis[11] or into triphosphates for enzymatic polymerization,[12] as well as on the polymeric level by post-modification of oligonucleotides, RNA, or DNA.[6a,13]

A promising approach to the spin labeling of oligonucleotides is the copper(I)-catalyzed Huisgen–Sharpless–Meldal alkyne–azide cycloaddition (CuAAC), the so-called 'click' reaction.[14] It has been proven to be an ideal bio-orthogonal protocol for ligating functional molecules to biological or nonbiological materials in organic and aqueous reaction systems.[15]

To avoid perturbation of the DNA structure, the click reaction is performed most efficiently when the ligand is introduced into the major groove of DNA. Consequently, 7-deazapurines have been used to modify the 7-position (purine numbering is used throughout the manuscript). Likewise, the 5-position of the pyrimidine base can be used for the same purpose.[16] Our laboratory has made many contributions to this field over the years.[17] Recently, it was shown that reporter groups of moderate size can be introduced into the major groove of B-DNA by the CuAAC reaction.[18]

Herein we report on the synthesis of oligonucleotides incorporating a derivative of 7-deaza-2′-deoxyadenosine (**1**) or 2′-deoxyuridine (**2**) bearing ethynyl side-chains and their post-modification with nitroxide labels (Figure 1).[19] For this purpose, phosphoramidites of nucleosides **1** and **2** were synthesized and employed in solid-phase synthesis. The post-synthetic functionalization of the oligonucleotides by 'click' chemistry was performed with 4-azido-2,2,6,6-tetramethylpiperidine 1-oxyl (**3**, 4-azido-TEMPO) (Scheme 1). For comparison, the reaction was studied on the nucleoside level, which yielded conjugates **4** and **5**. Two TEMPO residues were introduced at distant positions of a single-stranded oligonucleotide. Furthermore, a TEMPO residue was also 'clicked' to each nucleobase of a modified 'dA-dT' base pair within an oligonucleotide duplex incorporating the nucleosides **1** and **2**. For both approaches, distance measurements were performed by using cw and pulse EPR spectroscopy.

Results and Discussion

Synthesis and properties of the monomers: 7-Deaza-7-ethynyl-2′-deoxyadenosine (**1**) has already been synthesized[19] but has not been incorporated into oligonucleotides, whereas the incorporation of nucleoside **2** in oligonucleotides has

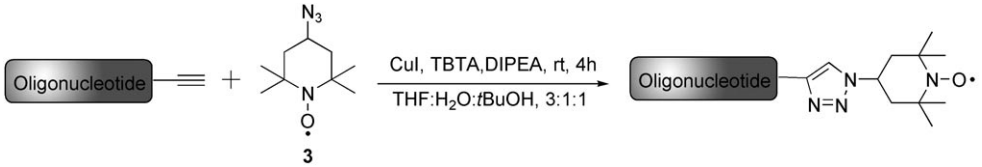

Scheme 1. Cu^{I}-catalyzed alkyne–azide cycloaddition 'click' reaction. TBTA = tris(benzyltriazolylmethyl)amine; DIPEA = *N*,*N*-diisopropylethylamine.

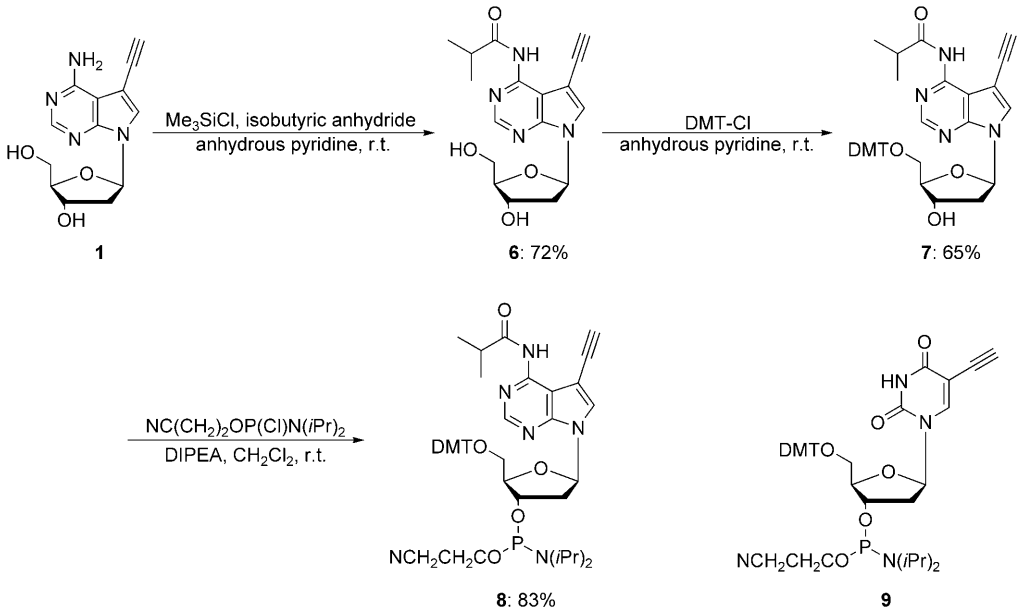

Scheme 2. Synthesis of phosphoramidite building block **8**. DMT-Cl = 4,4′-dimethoxytrityl chloride.

previously been described.[16] Herein, we report the conversion of nucleoside **1** into the phosphoramidite building block **8**, which was employed in solid-phase oligonucleotide synthesis. For amino group protection of nucleoside **1**, the isobutyric residue was chosen[17a] and transient protection was employed to give **6** in a yield of 72% (Scheme 2). Compound **6** was converted into the DMT derivative **7** under standard conditions in a yield of 65%. Phosphitylation with 2-cyanoethyl *N*,*N*-diisopropylchlorophosphoramidite furnished the phosphoramidite **8** in a yield of 83% (Scheme 2). The phosphoramidite **9** was prepared according to a published procedure.[16]

Next the click reaction was performed on nucleosides **1** and **2** with 4-azido-2,2,6,6-tetramethylpiperidine 1-oxyl (**3**, 4-azido-TEMPO). The paramagnetic radical, which contains an unpaired electron and a 'clickable' azido function, was synthesized from 4-hydroxy-2,2,6,6-tetramethylpiperidine 1-oxyl according to a literature procedure.[20] Then the 7-ethynyl nucleosides **1** and **2** were functionalized with **3** by the click reaction to give the conjugates **4** and **5**, respectively, in the presence of CuI in a 3:1:1 mixture of THF/*t*BuOH/H_2O (Scheme 3). The addition of *N*,*N*-diisopropylethylamine (DIPEA) was essential for the completion of the reaction within 4 h. CuI has been used as the copper(I) source instead of the $Cu^{II}SO_4$/ascorbic acid system to avoid reduction of the nitroxide radical by ascorbic acid to the nonparamagnetic hydroxylamine derivative during the click reaction.[10,21] The spin-labeled 1,2,3-triazolyl nucleoside conjugate **4** was obtained in a yield of 64%, whereas **5** was formed in a yield of 55%.

All compounds were characterized by UV, ^1H, and ^{13}C NMR spectroscopy, mass spectrometry, and elemental analysis (see the Experimental Section, Table 2, and the

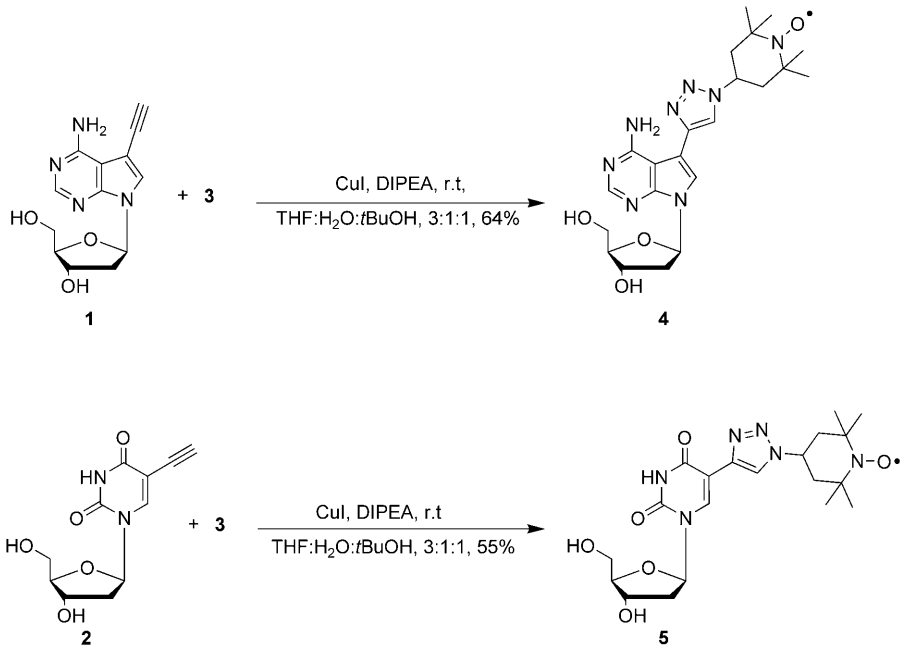

Scheme 3. Functionalization of nucleosides **1** and **2** with 4-azido-TEMPO (**3**).

Supporting Information). All the ^{1}H NMR signals of the spin-labeled compounds are broadened and furthermore some atoms of the TEMPO residue do not appear in either the ^{1}H or the ^{13}C NMR spectra. The signal intensities of the peaks obtained for the triazole moiety and partially for the nucleobase are also affected.[22] The monomeric spin-labeled conjugates **4** and **5** were analyzed by EPR spectroscopy to confirm the presence of the intact nitroxide label (data not shown).

Synthesis and characterization of the oligonucleotides for spin labeling: A series of oligonucleotides were synthesized (see Table 1). After cleavage from the solid support, the oligonucleotides were deprotected according to the standard procedure (25% aq. NH_3, 60°C, 14–16 h). However, in the case of oligonucleotides containing 5-ethynyl-2′-deoxyuridine (**2**), significant amounts of byproducts were formed during the deprotection with ammonia at elevated temperature (55°C, 14–16 h). As the impurity shows a similar mobility in HPLC as the target molecule, it was necessary to change the deprotection conditions to room temperature (25% aq. NH_3, 12 h). Consequently, tBPA-protected phosphoramidites were used.[23] The oligonucleotides were detritylated and purified by reversed-phase HPLC. The homogeneity of the oligonucleotides was confirmed by reversed-phase HPLC as well as by MALDI-TOF mass spectrometry (see the Supporting Information). The base compositions of the oligonucleotides containing **1** and **2** were determined by enzymatic hydrolysis with snake venom phosphodiesterase followed by alkaline phosphatase and subsequent reversed-phase HPLC chromatography (see the Supporting Information).

Previously it was reported by our laboratory that the various 5-alkynylpyrimidines and 7-alkynylated 7-deazapurines increase duplex stability by 1–3°C per modification.[18,24] In this work we studied the impact of the ethynyl side-chain of nucleosides **1** and **2** on duplex stability (Table 1). For this, the oligonucleotide duplex 5′-d(TAGGTCAATACT)-3′ (**10**)·3′-d(ATCCAGTTATGA)-5′ (**11**) was used as reference. To be consistent with the conditions used in low-temperature EPR experiments, 10% glycerol (cryoprotectant) was added to the buffer solution for all the T_m measurements. From Table 1 it can be seen that the replacement of a dA residue by 7-deaza-7-ethynyl-2′-deoxyadenosine (**1**) has a positive effect on duplex stability ($T_m = 44$°C for **12·11**). This effect is more pronounced when multiple positions are modified with nucleoside **1** (**14·11**, $\Delta T_m = 2$°C per modification). According to Table 1, the replacement of one dT residue by 5-ethynyl-2′-deoxyuridine (**2**) has a marginal influence on duplex stability ($T_m = 43$°C for duplex **10·13**). A similar result was obtained with the duplex **12·13**, which contains one 'dA-dT' base pair modified with ethynyl-substituted residues.

The thermal stability of the duplexes in 0.1 M NaCl buffer with or without glycerol (data in parentheses) was compared and revealed significant destabilization (**10·11**, **12·11**, and **10·13**). These results are in agreement with previous work[25] in which it was found that glycerol reduces the thermal stability of duplexes by decreasing the number of water molecules interacting with oligonucleotide solvation sites. This alters the electrostatic interactions within the polynucleotide chain and its surrounding counter-ion. The influence of the spin label on duplex stability (oligonucleotide duplexes containing **4** or **5**) will be discussed later.

Table 1. T_m values of oligonucleotide duplexes containing ethynylated nucleosides and spin-labeled conjugates.[a]

Duplex	T_m [°C]	ΔT_m [°C]	$\Delta G°_{310}$ [kcal mol^{-1}][b]
5′-d(TAG GTC AAT ACT) (**10**) 3′-d(ATC CAG TTA TGA) (**11**)	43(47)	–	−9.7
5′-d(TAG GTC **1**AT ACT) (**12**) 3′-d(ATC CAG TTA TGA) (**11**)	44(47)	+1	−9.9
5′-d(TAG GTC AAT ACT) (**10**) 3′-d(ATC CAG **2**TA TGA) (**13**)	43(46)	0	−9.5
5′-d(TAG GTC **1**AT ACT) (**12**) 3′-d(ATC CAG **2**TA TGA) (**13**)	43	0	−9.2
5′-d(TAG GTC **1**AT **1**CT) (**14**) 3′-d(ATC CAG TTA TGA) (**11**)	47	+4	−10.6
5′-d(TAG GTC **4**AT ACT) (**15**) 3′-d(ATC CAG TTA TGA) (**11**)	40[c]	−3	−8.6
5′-d(TAG GTC AAT ACT) (**10**) 3′-d(ATC CAG **5**TA TGA) (**16**)	42[c]	−1	−9.3
5′-d(TAG GTC **4**AT ACT) (**15**) 3′-d(ATC CAG **5**TA TGA) (**16**)	37	−6	−8.0
5′-d(TAG GTC **4**AT **4**CT) (**17**) 3′-d(ATC CAG TTA TGA) (**11**)	41[c]	−2	−8.7

[a] Measured at 260 nm in 0.1 M NaCl, 10 mM $MgCl_2$, and 10% glycerol (pH 7.0) at 5 μM single-strand concentration. Data in parentheses were measured in 0.1 M NaCl and 10 mM $MgCl_2$ buffer (pH 7.0) without glycerol. [b] $\Delta G°_{310}$ values were determined from the melting curves by using the software MELTWIN, version 3.0 (J. A. McDowell, **1996**). The $\Delta G°_{310}$ values are given to within an error of ±15%. [c] 10% excess of the unmodified sequence.

Introduction of nitroxide labels into the oligonucleotides: Of the synthetic strategies available for introducing spin labels into oligonucleotides, spin-labeled phosphoramidites have already been employed in solid-phase oligonucleotide synthesis.[11] Other approaches use backbone labeling. Either hydrogen phosphonates or phosphorothioates are incorporated into the phosphodiester chain selectively and are then labeled afterwards with appropriately functionalized spin-labeled derivatives.[13b,26] Because phosphorothioates prepared under standard conditions are diastereomeric, spin-labeled conjugates with an R_P or S_P configuration located in different environments of the DNA chain are formed. Another possibility is the application of thiooxo nucleosides as spin-label targets, for example, 4-thiouridine or 6-thioguanosine as target sites that are functionalized with methanethiosulfonate spin labels.[27] However, this approach is restricted to

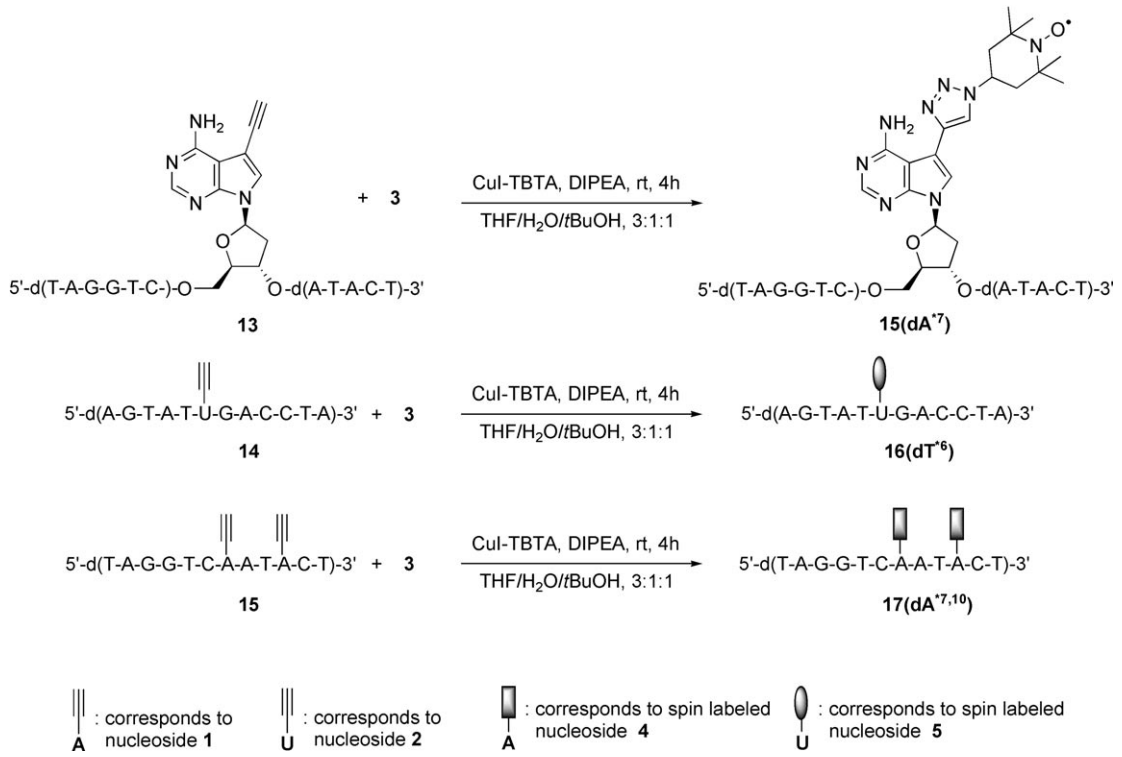

Scheme 4. Oligonucleotides labeled with 4-azido-TEMPO (**3**) by the click reaction. The abbreviations dA*[7], dT*[6], and dA*[7,10] correspond to the modified nucleoside (**4** or **5**) and its position within the oligonucleotide sequence indicated by the superscript number.

nucleobases in which oxygen can be replaced by sulfur, for example, 2′-deoxyuridine or -guanosine. The resulting S–S bridges were obtained in high yields, but cleavage of the disulfide was observed over longer periods of time.[27] Another common protocol uses the Sonogashira cross-coupling reaction performed on a CPG resin used for solid-phase oligonucleotide synthesis. In this case, fairly rigid spin labels were introduced into oligonucleotides.[6a,13d]

As we wanted to develop an efficient and universal protocol for spin labeling, this manuscript reports for the first time the use of the CuAAC 'click' reaction for direct oligonucleotide spin labeling using nucleobases as target sites. This approach has the following advantages: 1) The simultaneous incorporation of two spins or even more labels in a highly efficient way, 2) spin labeling can be accomplished at different nucleobases within one oligonucleotide strand, 3) the target sites for spin labeling (nucleosides **1** and **2**) within one particular oligonucleotide can also be used for the introduction of other reporter groups, for example, for FRET studies, and 4) accumulated information relating to structural changes can be collected by direct comparison of data obtained from the various labels introduced at identical positions by using one particular oligonucleotide for post-modification. The click method, which is presented below, can be performed on free oligonucleotides in solution, but is also applicable to solid-support-bound oligonucleotides.

Oligonucleotides with ethynyl-substituted nucleosides **1** or **2** were functionalized with 4-azido-TEMPO (**3**) in solution to produce paramagnetic oligonucleotides. The reactions were carried out in aqueous THF/H_2O/*t*BuOH (3:1:1) at room temperature in the presence of the chelate ligand of CuI–TBTA [tris(benzyltriazolylmethyl)amine] and *N*,*N*-diisopropylethylamine (DIPEA; Scheme 4). Owing to the delicate nature of the nitroxide, no reducing reagent was used during the 'click' reactions to form the oligonucleotide conjugates. Monitoring the click reactions by HPLC showed that the starting materials were completely consumed after 4 h (Figure 2 and the Supporting Information). Labeled oligonucleotides were further purified by reversed-phase HPLC (RP-18 column). The formation of click products was confirmed by MALDI-TOF mass spectrometry and enzymatic hydrolysis (see the Supporting Information).

As discussed above, the ethynyl substituents of nucleosides **1** and **2** have a negligible influence on DNA stability. The short alkynyl side-chain (2–3 Å), which is shorter than the depth of the B-DNA major groove (8.8 Å),[2] increases base-pair stability only slightly (Table 1). To evaluate the influence of the bulky spin-label modification on duplex stability, the oligonucleotides incorporating the functionalized residues **4** and **5**, both carrying a spin label, were investigated (Table 1). A single incorporation of the 7-deazapurine conjugate **4** at a central position [**15**(**dA***[7])·**11**] slightly destabilizes the 'dA-dT' base pair by 3 °C, whereas the incorporation of two conjugates of **4** [**17**(**dA***[7,10])·**11**] does not destabilize the duplex further (−1 °C per modification). A similar trend was observed with the 5-substituted 2′-deoxyuridine conjugate **5** (**10**·**16**(**dT***[6]), $\Delta T_m = -1$ °C). Note that for duplex **15**(**dA***[7])·**16**(**dT***[6]) with a spin-labeled 'dA-dT' base

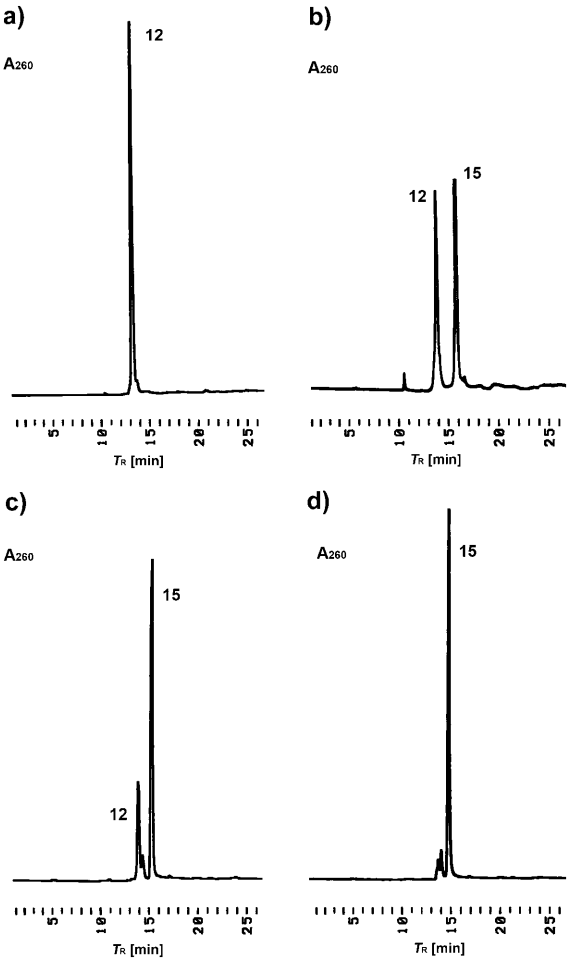

Figure 2. HPLC profiles of the Cu^{I}-catalyzed 'click' reaction of the oligonucleotide 5′-d(TAG GTC **1**AT ACT) (**12**) with 4-azido-TEMPO (**3**) monitored at intervals by HPLC: 20 μL reaction mixture per injection after a) 0, b) 60, c) 120, and d) 240 min. Gradient: 0–30 min 0–60% B in A, 30–40 min 60% B in A, 60–0% B in A, flow rate 0.7 mL min^{-1} (A = 0.1 M $(Et_3NH)OAc$ (pH 7.0)/MeCN (95:5), B = MeCN).

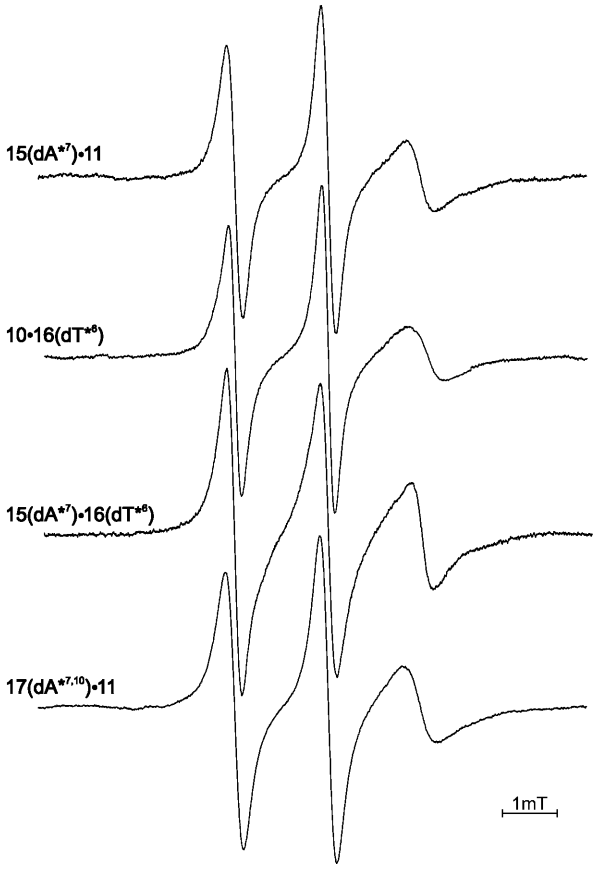

Figure 3. Room-temperature (T = 298 K) cw EPR spectra (9.4 GHz) of single- and double-labeled samples measured in 0.1 M NaCl, 10 mM $MgCl_2$, and 10% glycerol (pH 7.0). All plots are normalized by amplitude.

pair, the T_m value is lowered by 6 °C. The above results clearly demonstrate that a single bulky spin label at the 7-position of a 7-deazapurine or the 5-position of a pyrimidine does not disturb the DNA duplex structure due to the non-critical position of the spin label (C-7 of 7-deazapurine and C-5 of pyrimidine). However, when two spin labels are introduced at both sides of a 'dA-dT' base pair, the helix structure is slightly perturbed as reflected by the decrease in T_m (Table 1). The base pair is not destroyed as such a phenomenon would lead to a more significant decrease in the value of T_m (ΔT_m = 10–15 °C).

EPR analysis of the spin-labeled oligonucleotides: As melting temperature data cannot answer questions relating to nanoscale changes, EPR distance measurements were undertaken. In this regard, oligonucleotide duplexes with spatially isolated TEMPO residues or with nitroxides linked to each site of a base pair were investigated by cw and pulse EPR spectroscopy. The room-temperature spectra of the single- and double-labeled oligonucleotides are compared in Figure 3. All the spectra indicate a high mobility of the spin-labeled side-chains and the presence of only one distinct motional component; the reorientational freedom of the spin-labeled side-chains is not restricted by their immediate microenvironment. Interestingly, for the modified duplex **15**-(**dA**^{*7})•**16**(**dT**^{*6}), the amplitudes of the signals decrease from the low-field to the high-field peaks. In addition, considerable broadening of the lines of the spectra of the double-labeled strand relative to the spectra of the single-labeled strand is evident and is a result of spin–spin interactions. Although the double-labeled duplex **15**(**dA**^{*7})•**16**(**dT**^{*6}) reveals this anisotropic behavior, the single-labeled duplexes **15**-(**dA**^{*7})•**11** and **10**•**16**(**dT**^{*6}) do not display such properties. Given that the anisotropic behavior is not caused by the constraints of neighboring nucleobases, the anisotropy provides evidence of steric interactions between the two spin-labeled side-chains or of a slightly perturbed 'dA-dT' base pair. The perturbation of the DNA structure has already been indicated by the lower T_m value (ΔT_m = −6 °C; Table 1). In contrast, the room-temperature spectrum of the modified duplex with distant spin labels **17**(**dA**^{*7,10})•**11** does not exhibit any anisotropic behavior. No perturbation of the DNA structure caused by spin labeling and no interaction of

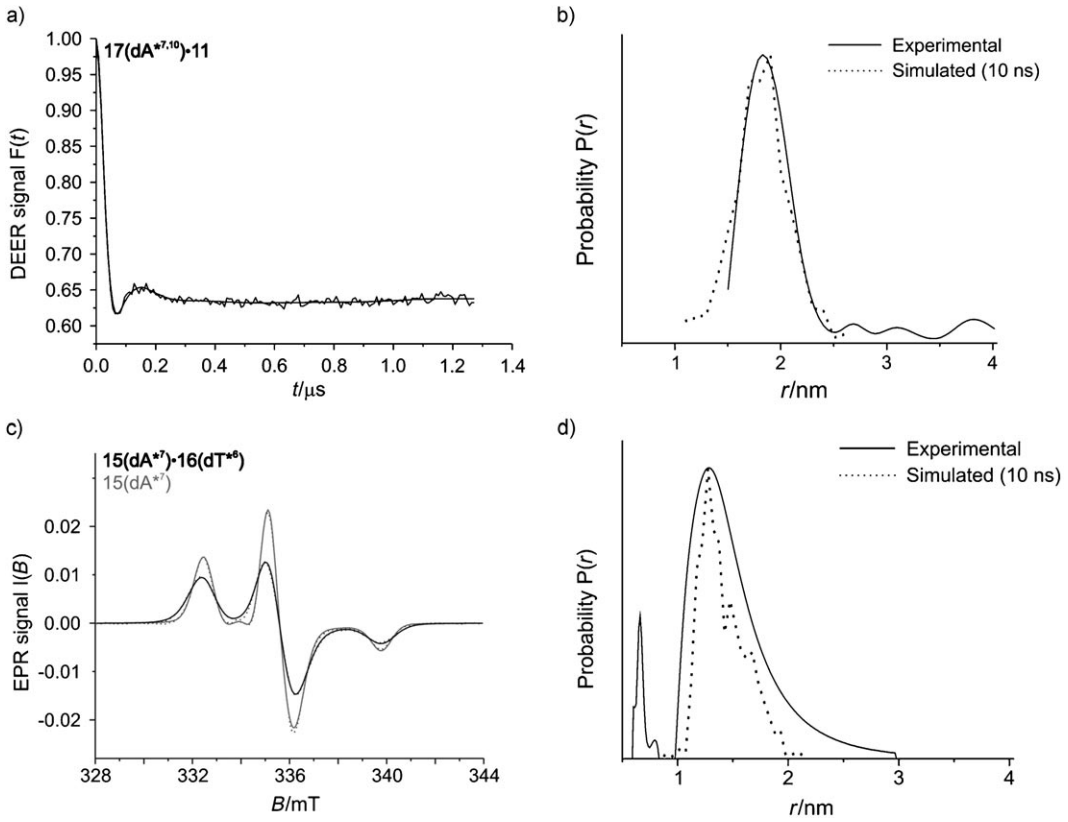

Figure 4. Low-temperature ($T=50$ K) DEER spectra of spin-labeled duplex **17(dA*^{7,10})·11** (9.4 GHz). a) Background-corrected dipolar evolution data $F(t)$. b) Comparison of the distance distributions $P(r)$ obtained by Tikhonov regularization[33] of the pulse EPR spectrum (solid line) and simulated interspin distances using YASARA Dynamics (dotted line). c) Low-temperature ($T=160$ K) cw EPR powder spectra recorded at the X-band frequency. Experimental spectra of double-labeled DNA duplex **15(dA*^{7})·16(dT*^{6})** (black solid line) and single-labeled oligonucleotide **15(dA*^{7})** (grey solid line). The corresponding simulated EPR spectra are represented by dashed lines. All plots are normalized by spin number. d) Comparison of the distance distributions $P(r)$ obtained by Tikhonov regularization (ShortDistances)[31] of the cw EPR spectrum (solid line) and interspin distances using YASARA Dynamics[34] (dotted line). All experiments were performed in 0.1 M NaCl, 10 mM $MgCl_2$, and 10% glycerol (pH 7.0). Distance distributions are normalized by amplitude.

the two spin labels are observable in the spectrum, which is not unexpected because the two spin labels are at a distance.

The results of the cw and DEER measurements performed at 160 and 50 K, respectively, are depicted in Figure 4. Tikhonov regularization of the DEER data for the double-labeled duplex **17(dA*^{7,10})·11** reveals a well-defined single distance population with an interspin distance of 1.8 ± 0.2 nm (Figure 4b). The distance distribution width of 0.2 nm is narrow, half of the width found for an analogous labeled DNA duplex reported by Flaender et al.[28] In fact, it is similar to a DNA duplex system with 4-amino-TEMPO attached to 2-fluorohypoxanthine bases.[5] Hence the presented DNA system, spin-labeled by the click reaction, is a powerful tool for measuring accurate interspin distances and is sensitive even to small structural changes. Furthermore the rigid spin label will allow orientation-selective studies to obtain the relative orientation of both spin labels as demonstrated by Schiemann et al.[29]

The data obtained for the double-labeled duplex **15-(dA*^{7})·16(dT*^{6})** reveal an interspin distance below the accessible distance range of DEER spectroscopy (<1.5 nm;[30] data not shown). Therefore we used cw EPR spectroscopy at 160 K to determine the interspin distance for **15-(dA*^{7})·16(dT*^{6})**. No dipolar broadening was observed for the single-stranded oligonucleotide **15(dA*^{7})**, which is taken as a reference for the simulation of dipolar broadening. In contrast, the experimentally observed spectrum of **15-(dA*^{7})·16(dT*^{6})** exhibits significant dipolar broadening (Figure 4c). Fitting of the simulated dipolar broadened EPR spectrum (Figure 4c, dashed line) to the experimental spectrum by using the Tikhonov regularization approach provided by the ShortDistances program[31] yielded a mean interspin distance of 1.4 ± 0.3 nm and a fraction of the single spin-labeled component of 11% (Figure 4d, solid line). In addition, the data were fitted with the DipFit program[32] in which a sum of the Gaussian distributions of interspin distances is assumed. This results in a distance distribution centered at 1.4 ± 0.1 nm and an A_{zz} value of 3.7 mT. The fraction of the single spin-labeled component amounts to 10%. The high A_{zz} value indicates a high polarity in the immediate microenvironment of the spin-labeled side-chains. Hence the spin-labeled side-chains are accessible to water molecules, which is in agreement with the DNA model

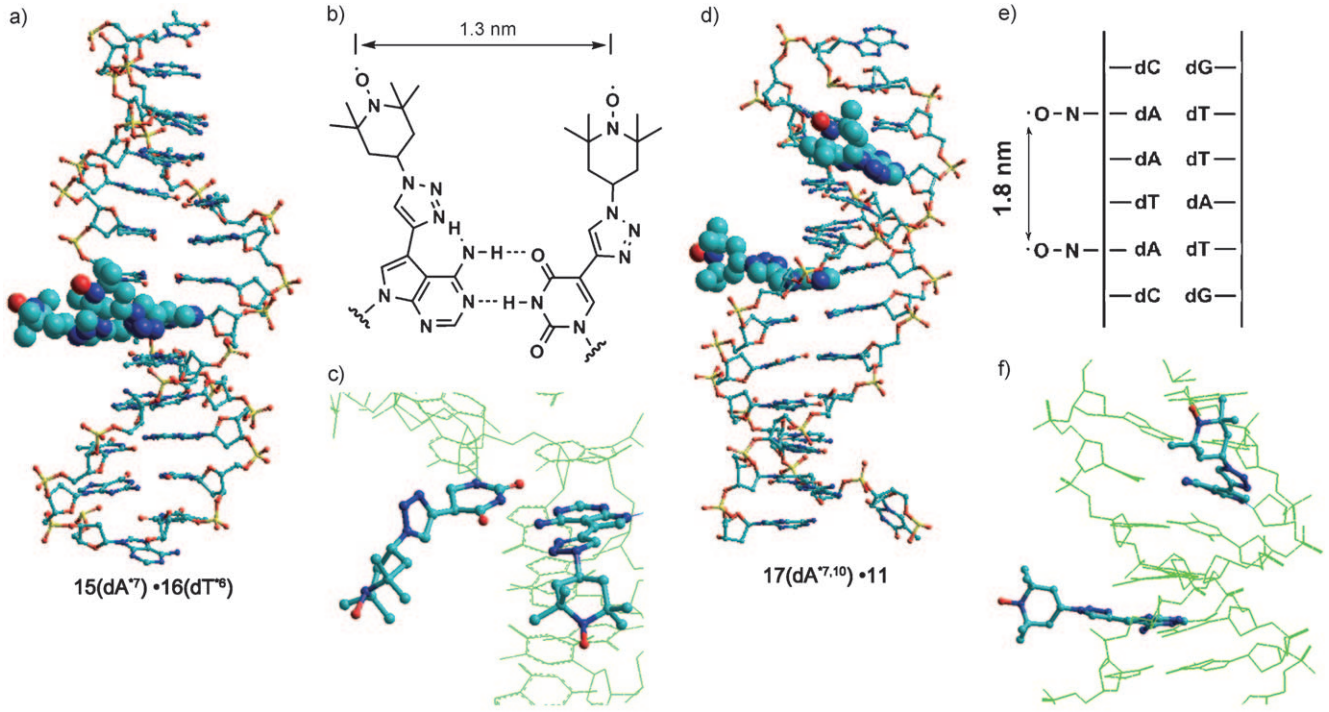

Figure 5. Molecular dynamics (MD) simulation snapshots of the DNA duplexes **15**(**dA***[7])·**16**(**dT***[6]) and **17**(**dA***[7,10])·**11**. The MD simulations were performed by using the AMBER99 force field implemented in YASARA Dynamics.[34] a) MD simulation snapshot of DNA duplex **15**(**dA***[7])·**16**(**dT***[6]). b) Modified base pair of **4** and **5** and the spin-label distance, determined for the oxygen atoms of the nitroxides. c) MD simulation snapshot of the spin-labeled 'dA-dT' base pair. d) MD simulation snapshot of DNA duplex **17**(**dA***[7,10])·**11**. e) Spin–spin distance for **17**(**dA***[7,10])·**11** containing two spin labels within one of the strands, determined for the oxygen atoms of the nitroxides. f) MD simulation snapshot of duplex **17**(**dA***[7,10])·**11**.

(Figure 5). The high spin-labeling efficiency is reflected by the minor single-labeled fraction of 10–11 %.

From the point of view of physical measurements, a spin label should be rather rigid and not show significant independent movement with regard to the DNA duplex. Short alkynyl linkers[6a,11a] or phenoxazine moieties[22b] fulfill these requirements. However, rigid and bulky spin labels affect the DNA structure. They can stabilize or destabilize base pairs and provide a 'more or less' altered picture of the 'real' DNA duplex structure. On the other hand, a more flexible spin label is prone to independent movements but has a smaller influence on the duplex structure. Hence a suitable compromise has to be found between the ease of synthesis, the universal character of the protocol, the rigidity of the label, and the steric perturbation of the DNA structure induced by the label. We believe that spin labeling using CuAAC to afford spin labels linked through an *s*-1,2,3-triazole moiety fulfills most of these requirements. This is supported by the very small linewidths of the signals obtained from DEER measurements.

Comparison with molecular dynamics simulation: To analyze the effects induced by spin labeling on the duplex structure and to provide a more comprehensive description, molecular dynamics (MD) simulations were performed on the DNA duplexes **15**(**dA***[7])·**16**(**dT***[6]) and **17**(**dA***[7,10])·**11**. As a starting structure both models were built with spin labels adjusted to their experimentally determined distance by using YASARA Dynamics (see the Experimental Section for details).[34]

For duplex **15**(**dA***[7])·**16**(**dT***[6]), the spin label leads to a marginal perturbation of the spin-labeled 'dA-dT' base pair during the MD simulation. At the same time, the overall structure and in particular the base pair remains stable during the whole MD simulation of 10 ns, as depicted in Figure 5. The experimental cw EPR spectrum of **15**(**dA***[7])·**16**(**dT***[6]) at room temperature indicates either a steric interaction between the two spin-labeled side-chains or a disturbed 'dA-dT' base pair. On the basis of the MD simulation, we can exclude a disturbed base pair and conclude that steric interactions lead to the anisotropic characteristics of the spectrum. For **15**(**dA***[7])·**16**(**dT***[6]), the simulated mean interspin distance is centered at 1.3 ± 0.2 nm, as shown in Figure 4d (dotted line) and Figure 5b. Thus, there is reasonable agreement between the experimental and simulated interspin distance distributions with a slight shift of the simulated interspin distance to shorter distances. Analysis of the data for duplex **17**(**dA***[7,10])·**11** exhibits an experimentally determined interspin distance of 1.8 ± 0.2 nm and a simulated mean interspin distance of 1.8 ± 0.2 nm (Figure 4b and Figure 5e). The agreement between the simulated and experimental interspin distance distributions is excellent, both for the interspin distances and the widths of the distributions.

Conclusion

In this study the TEMPO spin label was introduced into DNA nucleobases **1** and **2** by the copper-assisted azide–alkyne 'click' reaction. In this way a 'dA-dT' base pair was generated with one spin label linked to each nucleobase. In addition, one strand of a DNA duplex was modified with two spin labels at distant positions. Both post-modification reactions occurred with high efficiency. The spin-labeling protocol performed on the two ethynylated DNA constituents **1** (dA*) and **2** (dU*) can be extended to dG and dC derivatives, making all four DNA constituents, two pyrimidine bases and two purine bases in the form of 7-deazapurines, accessible. No steric interaction between the two distant spin labels was observed but a negligible perturbation of the DNA structure was noted [duplex **17**(**dA*^{7,10}**)·11**]. However, steric interactions between the spin labels and a small DNA structure perturbation were observed when two spin labels were linked to the 'dA-dT' base pair. By cw and pulse EPR spectroscopy, we determined mean interspin distances of (1.4 ± 0.3) nm for **15**(**dA*^{7}**)·16**(**dT*^{6}**) and (1.8 ± 0.2) nm for **17**(**dA*^{7,10}**)·11**. For the two spin labels in more distant positions, the determined distance distribution is exceptionally narrow and suitable for the identification of even small structural changes. Hence the spin-labeled DNA system obtained by the 'click' reaction will allow us to obtain detailed insights into the structural changes caused to DNA structures by mispairing, DNA damage, and/or lesions. Moreover, the target sites for spin labeling (ethynylated nucleosides **1** and **2**) within one particular oligonucleotide can also be used for the introduction of other reporter groups. Accumulated information regarding structural DNA/RNA changes can be collected by direct comparison of data obtained from the various labels. For this reason, the click approach has advantages over other protocols described earlier.

Experimental Section

General: All chemicals were purchased from Acros, Aldrich, Sigma, or Fluka (Sigma–Aldrich Chemie GmbH, Deisenhofen, Germany). Solvents were of laboratory grade. Thin-layer chromatography (TLC) was performed on TLC aluminium sheets covered with silica gel 60 F254 (0.2 mm, VWR International, Germany). Flash column chromatography (FC) was performed on silica gel 60 (VWR International, Darmstadt, Germany) at 0.4 bar. UV spectra were recorded on a Hitachi U-3000 spectrophotometer. λ_{max} and ε values are given in nm and $dm^3 mol^{-1} cm^{-1}$, respectively. NMR spectra were recorded on a Bruker DPX 300 spectrometer at 300 MHz for ^{1}H and 75 MHz for ^{13}C NMR spectroscopy (see Table 2). δ values are in ppm relative to Me_4Si as the internal standard for ^{1}H and ^{13}C NMR or relative to 85% H_3PO_4 as the external standard for ^{31}P NMR; J values are given in Hz. For NMR spectra recorded in DMSO, the chemical shift of the solvent peak was set to 2.50 ppm for ^{1}H NMR and 39.50 ppm for ^{13}C NMR. Elemental analyses were performed by the Mikroanalytisches Laboratorium Beller, Göttingen (Germany). Reversed-phase HPLC was carried out on a 4×250 mm RP-18 (10 mm) LiChrospher 100 column (VWR International) with a Merck-Hitachi HPLC pump (Model L-6250) connected with a variable wavelength monitor (model 655A), a controller (model L-500), and an integrator (model D-2500).

Oligonucleotide synthesis, purification, and characterization: The oligonucleotides were synthesized with a DNA synthesizer, model 392–08 (Applied Biosystems, Weiterstadt, Germany), on a 1 μmol scale starting from the phosphoramidite **8** following the synthesis protocol for 3′-(2-cyanoethyl phosphoramidites) (User's Manual for the 392 DNA synthesizer, Applied Biosystems, Weiterstadt, Germany). Oligonucleotides containing 5-ethynyl-2′-deoxyuridine (**2**) were prepared by using the corresponding phosphoramidite **9** and a fast deprotection procedure.[16] For this purpose, 4-*tert*-butylphenoxyacetyl-protected canonical phosphoramidites (Millipore) and the capping reagent 4-*tert*-butylphenoxyacetic anhydride instead of acetic anhydride were used. The coupling efficiency was always higher than 95%. After cleavage from the support, the oligomers were incubated in a 25% aq. NH_3 solution. Reactions were performed at 60 °C for 14–16 h for oligonucleotides containing **1** and at room temperature for 12 h for oligonucleotides containing **2**. The 5′-*O*-dimethoxytrityl oligomers were purified by reversed-phase HPLC (Merck-Hitachi HPLC; RP-18 column; gradient system [A = 0.1 M $(Et_3NH)OAc$ (pH 7.0)/MeCN 95:5, B = MeCN]: 3 min 20% B in A, 12 min 20–50% B in A, and 25 min 20% B in A; flow rate = 1.0 mL min^{-1}). The purified 'trityl-on' oligonucleotides were treated with 2.5% $CHCl_2COOH/CH_2Cl_2$ for 5 min at 0 °C to remove the 4,4′-dimethoxytrityl residues. The detritylated oligomers were purified again by reversed-phase HPLC (gradient: 0–20 min 0–20% B in A; flow rate = 1 mL min^{-1}). The oligomers were desalted on a short column (RP-18, silica gel) and lyophilized in a Speed-Vac evaporator to yield colorless solids that were frozen at −24 °C. The melting temperature curves were measured with a Cary-100 Bio UV-VIS spectrophotometer (Varian, Australia) equipped with a Cary thermoelectric controller. The temperature was measured continuously in the reference cell with a Pt-100 resistor at a heating rate of 1 °C min^{-1}. The thermodynamic data for duplex formation were calculated by using the Meltwin 3.0 program. The oligonucleotides containing **1**, **2**, **4**, and **5** were enzymatically hydrolyzed with snake venom phosphodiesterase (EC 3.1.15.1, *Crotallus adamanteus*) and alkaline phosphatase (EC 3.1.3.1, *Escherichia coli* from Roche Diagnostics GmbH, Germany) in 0.1 M Tris–HCl buffer (pH 8.3) at 37 °C, as described previously.[17a] The hydrolysis product was analyzed by reversed-phase HPLC (RP-18). The constituents were quantified from the peak areas divided by the extinction coefficients ε_{260} of the nucleosides: dA 15400, dC 7300, dG 11700, dT 8800, **1** 11100 (MeOH), **2** 10500 (MeOH), **4** 10500 (MeOH), **5** 7600 (MeOH). MALDI-TOF mass spectra were recorded in the linear negative mode with an Applied Biosystems Voyager DE PRO spectrometer with 3-hydroxypicolinic acid (3-

Table 2. ^{13}C NMR chemical shifts (δ) of the alkynylated nucleosides and spin-labeled derivatives.[a,b]

	C-2[c] C-2[d]	C-4[c] C-6[d]	C-4a[c] C-5[d]	C-5[c] C-7[d]	C-6[c] C-8[d]	C-7a[c] C-4[d]	C≡C	Triazole	C-1′	C-3′	C-4′	C-5′	C=O	$(MeO)_2$Tr
1[19]	152.7	157.5	102.3	93.9	127.0	149.1	82.9, 77.3	–	83.2	70.9	87.5	61.8	–	–
2[35]	149.5	144.5	97.5	–	–	161.6	83.6, 76.4	–	84.7	69.9	87.5	60.7	–	–
4	152.3	157.7	106.0	99.6	119.1	150.3	–	142.7, 118.4[e]	82.3	70.8	87.1	61.9	–	–
5	149.3	135.8	105.2	–	–	160.8	–	139.6, 119.8[e]	84.5	70.3	87.3	61.2	–	–
6	151.6	151.6	111.3	96.2	131.2	151.1	82.1, 77.3	–	83.1	70.9	87.6	61.7	175.8	–
7	151.6	151.6	111.3	96.2	131.1	151.0	82.1, 77.1	–	83.1	70.6	85.5	64.1	175.8	55.0

[a] Measured in [D_6]DMSO at 298 K. [b] The signal of C-2' is superimposed by DMSO. [c] Systematic numbering. [d] Purine numbering. [e] Decreased signal intensity by spin label.

HPA) as matrix. The masses determined were identical to the calculated values (see the Supporting Information).

Preparation of oligonucleotides for EPR measurements: Lyophilized DNA samples were dissolved in 0.1 M NaCl, 10 mM $MgCl_2$, and 10% glycerol (pH 7.0) to yield a concentration of 60 μM for the single-stranded oligonucleotides and 60 μM for the DNA duplexes, respectively. Glycerol was added as a cryoprotectant during all low-temperature EPR experiments. For low-temperature cw and pulse EPR experiments, 30–40 μL of the sample solutions were used in EPR quartz capillaries with 4 and 3 mm outer diameters, respectively, and frozen in liquid nitrogen before insertion into the resonator. Sample volumes of 10 μL were loaded into EPR quartz capillaries with a 0.9 mm inner diameter for cw EPR measurements at room temperature.

EPR measurements: Room-temperature cw EPR spectra were recorded at X-band frequency with a Magnettech Miniscope MS200 X-band spectrometer equipped with a rectangular TE102 resonator. To avoid saturation and to obtain EPR spectra with a high signal-to-noise ratio, the microwave power was set to 10 mW and the B-field modulation amplitude was adjusted to 0.15 mT. Low-temperature cw EPR spectra for the determination of the interspin distance in the range of 1–2 nm were recorded at 160 K using a homemade X-band EPR spectrometer equipped with a Super High Sensitivity Probehead (Bruker). Temperature stabilization was achieved by a continuous flow helium cryostat (ESR 900, Oxford Instruments) in combination with a temperature controller (ITC 503S, Oxford Instruments). The microwave power was set at 0.2 mW and the B-field modulation amplitude adjusted to 0.25 mT. A B-NM 12 B-field meter (Bruker) allowed measurement of the magnetic field. The DEER experiments were performed at 50 K and X-band frequencies (9.4 GHz) with a Bruker Elexsys 580 spectrometer equipped with a 3 mm split ring resonator (ER 4118X-MS3, Bruker). The resonator was overcoupled at $Q \approx 100$ as measured by using the Xepr software (Bruker). A continuous flow cryostat (ESR900, Oxford Instruments) in combination with a temperature controller (ITC 503S, Oxford Instruments) was used for temperature stabilization. The following four-pulse DEER sequence was used:[36]

$$\pi/2(\upsilon_{obs})-\tau_1-\pi(\upsilon_{obs})-t'-\pi(\upsilon_{pump})-(\tau_1+\tau_2-t')-\pi(\upsilon_{obs})-\tau_2-\text{echo}$$

A two-step phase cycling ($+<X>$, $-<X>$) was realized on $\pi/2(\upsilon_{obs})$, whereas for all pulses at the observer frequency the $<X>$ channels were applied. The pump pulse had a length of 12 ns and the pump frequency υ_{pump} was positioned at the center of the resonator dip. This frequency corresponds to the maximum of the echo-detected nitroxide EPR absorption spectrum. The observer frequency υ_{obs} was set to the low-field local maximum of the absorption spectrum, which resulted in a 65 MHz offset with observer pulse lengths of 16 ns for $\pi/2$ and 32 ns for π pulses. Time t' was varied and τ_1 and τ_2 were kept constant. Deuterium modulation was averaged by adding traces at eight different τ_1 start values starting at $\tau_{1,0}=200$ ns and incrementing at $\Delta\tau_1=8$ ns. The dipolar evolution time is given by $t=t'-\tau_1$ and data with $t>0$ were analyzed.

Fitting of experimental cw EPR spectra: Fitting of the simulated dipolar broadened cw EPR spectra to the experimental spectra recorded at temperatures below 200 K revealed average interspin distances in the range of 1–2 nm, as described before by using the DipFit[32] or ShortDistances program.[31] The Heisenberg exchange interaction does not lead to significant distance errors as long as the through-space distances exceed 1.0 nm.[8,32] However, for distances below 1.0 nm or in case exchange is facilitated through bonds connecting the nitroxides, the effects of exchange interactions have to be considered. DipFit determines the best-fit parameters for the interspin distances and the distance distributions on the basis of a Gaussian distribution of distances. During the fitting procedure, the g tensor values, the A_{xx} and A_{yy} values of the hyperfine tensor, and the Lorentzian and Gaussian linewidth parameters are fixed to the values found for the reference spectra **16(dA*[7])**. In detail, A_{xx} and A_{yy} were fixed to 0.68 and 0.66 mT, respectively, whereas A_{zz} is variable. The g tensor values are set to $g_{xx}=2.0082$, $g_{yy}=2.0070$, and $g_{zz}=2.0022$. The EPR spectra are convoluted with a field-independent line-shape function composed of a superposition of 28% Lorentzian and 72% Gaussian of 0.51 and 0.42 mT widths, respectively. The fraction of the single spin-labeled component is variable. The interspin distance distribution is calculated by Tikhonov regularization using the ShortDistances program.[31] The interspin distance as well as the width and the fraction of the single spin-labeled component are adjustable during the fitting procedure.

Analysis of the DEER data: Analysis of the DEER data revealed interspin distances in the range of 1.5–8 nm based on the dipolar coupling frequency of dipolar coupled spins. The lower limit of the DEER experiments depends on the excitation bandwidth of the pump pulse, which has to be larger than the dipolar coupling of the spins and is in our case 1.5 nm.[30] To elucidate only interspin distances within one nanoscopic object, the intermolecular background contribution has to be separated from the intramolecular contribution. Therefore the experimental echo decay was background-corrected by using a homogeneous three-dimensional spin distribution followed by normalization of the function. Finally, the interspin distance distributions were calculated by fitting the corrected dipolar evolution function using Tikhonov regularization as implemented in DEERAnalysis2006.[33]

Molecular dynamics simulations: The molecular dynamics (MD) simulations were performed by using the AMBER99 force field implemented in YASARA Dynamics[34] with periodic cell boundaries. A simulation cell was constructed with 12 Å real space around the DNA model and filled with water molecules and Na^+/Cl^- counter-ions at locations of the lowest/highest electrostatic potential during a cell neutralization and pK_a prediction experiment (pH 7.0). After an energy minimization run, the final 10 ns MD simulations were performed at 298 K with 1 fs time steps under constant pressure with intermolecular forces being calculated every 2 fs. Periodic boundary crossing of solute atoms was prevented by function solute drift. The interspin distances were extracted by using the macro MD analyses provided by YASARA Dynamics.

7-(2-Deoxy-β-D-*erythro*-pentofuranosyl)-4-(isobutyrylamino)-5-ethynyl-7*H*-pyrrolo[2,3-*d*]pyrimidine (6): Me_3SiCl (1.16 mL, 9.10 mmol) was added to a stirred solution of compound **1**[19] (274 mg, 1 mmol) in anhydrous pyridine (5 mL) at room temperature. After 45 min, isobutyric anhydride (1.16 mL, 7.38 mmol) was introduced and the solution was stirred for another 2 h. The mixture was cooled to 0 °C, diluted with H_2O (5 mL), and stirred for 10 min. After the addition of 12% aq. NH_3 (5 mL), stirring was continued for 1 h at room temperature. The solvent was evaporated and the residue purified by flash chromatography (FC; silica gel, column 10×3 cm, CH_2Cl_2/CH_3OH, 95:5). Compound **6** was isolated as a colorless solid (248 mg, 72%). $R_f=0.42$ (CH_2Cl_2/CH_3OH, 90:10); ^{1}H NMR (300 MHz, [D$_6$]DMSO, 25 °C): $\delta=1.14$ (s, 6H; 2 CH_3), 2.26 (m, 1H; 2′-H$_\alpha$), 2.58 (m, 1H; CH), 2.78 (m, 1H; 2′-H$_\beta$), 3.43 (m, 2H; 5'-H), 3.84 (m, 1H; 4'-H), 4.08 (s, 1H; C≡CH), 4.37 (m, 1H; 3'-H), 5.04 (t, ^3J(H,H) = 5.3 Hz, 1H; 5'-OH), 5.35 (d, ^3J(H,H) = 4.0 Hz, 1H; 3'-OH), 6.62 (t, ^3J(H,H) = 6.4 Hz, 1H; 1'-H), 8.12 (s, 1H; 6-H), 8.62 (s, 1H; 2-H), 10.21 ppm (s, 1H; NH); UV/Vis (MeOH): λ_{max} (ε) = 238 (53000), 278 nm (26000 $mol^{-1}m^3cm^{-1}$); elemental analysis calcd (%) for $C_{17}H_{20}N_4O_4$: C 59.29, H 5.85, N 16.27; found: C 59.03, H 5.84, N 16.35.

7-[2-Deoxy-5-*O*-(4,4′-dimethoxytrityl)-β-D-*erythro*-pentofuranosyl]-4-(isobutyrylamino)-5-ethynyl-7*H*-pyrrolo[2,3-*d*]pyrimidine (7): Compound **6** (241.1 mg, 0.7 mmol) was dried by repeated coevaporation with anhydrous pyridine (3×5 mL) before dissolving in anhydrous pyridine (5 mL). 4,4′-Dimethoxytrityl chloride (DMT-Cl; 284.6 mg, 0.84 mmol) was added in three portions to this solution. The remaining solution was stirred for 3 h at room temperature. The reaction was quenched by the addition of MeOH (2 mL) and the mixture was stirred for another 30 min. The reaction mixture was diluted with CH_2Cl_2 (2×10 mL), extracted with 5% aqueous $NaHCO_3$ (30 mL) followed by H_2O (40 mL), dried over Na_2SO_4, and then evaporated to dryness. Purification by FC (silica gel, column 15×3 cm, CH_2Cl_2/acetone, 95:5→90:10) gave a colorless foam of **7** (295 mg, 65%). $R_f=0.64$ (CH_2Cl_2/CH_3OH, 90:10); ^{1}H NMR (300 MHz, [D$_6$]DMSO, 25 °C): $\delta=1.15$ (s, 6H; 2 CH_3), 2.31 (m, 1H; 2′-H$_\alpha$), 2.67 (m, 1H; CH), 2.81 (m, 1H; 2′-H$_\beta$), 3.16 (m, 2H; 5'-H), 3.72 (s, 6H; OCH_3), 3.96 (m, 1H; 4'-H), 4.07 (s, 1H; C≡CH), 4.38 (m, 1H; 3'-H), 5.40 (d, ^3J-(H,H) = 4.5 Hz, 1H; 3'-OH), 6.62 (t, ^3J(H,H) = 6.6 Hz, 1H; 1'-H), 6.84 (m, 4H; Ar-H), 7.16–7.40 (m, 9H; Ar-H), 7.95 (s, 1H; 6-H), 8.60 (s, 1H; 2-H), 10.17 ppm (s, 1H; NH); UV/Vis (MeOH): λ_{max} (ε) = 235 (56000),

276 nm (18000 $mol^{-1}m^3cm^{-1}$); elemental analysis calcd (%) for $C_{38}H_{38}N_4O_6$: C 70.57, H 5.92, N 8.66; found: C 70.32, H 5.82, N 8.70.

7-[2-Deoxy-5-*O*-(4,4′-dimethoxytrityl)-β-D-*erythro*-pentofuranosyl]-4-(isobutyrylamino)-5-ethynyl-7*H*-pyrrolo[2,3-*d*]pyrimidin-3′-(2-cyanoethyl)-*N*,*N*-diisopropylphosphoramidite (8): Compound **7** (259 mg, 0.4 mmol) was dissolved in anhydrous CH_2Cl_2 (3.0 mL) under argon and 2-cyanoethyl *N*,*N*-diisopropylchlorophosphoramidite (185 μL, 0.78 mmol) and *N*,*N*-diisopropylethylamine (150 μL, 0.87 mmol) were added at room temperature. After stirring for 20 min, the reaction mixture was diluted with CH_2Cl_2 and washed with 5% aq. $NaHCO_3$ followed by brine. The organic layer was separated, dried over anhydrous Na_2SO_4, filtered, and evaporated to dryness. The residue was dissolved in CH_2Cl_2 (1 mL) and purified by FC (column 4×10 cm, CH_2Cl_2/acetone, 9:1) to yield **8** (287.8 mg, 83%) as a colorless foam; R_f=0.44 (CH_2Cl_2/acetone, 70:10); ^{31}P NMR (121.5 MHz, $CDCl_3$, 25°C): δ=148.87, 148.70 ppm.

4-Amino-7-(2-deoxy-β-D-*erythro*-pentofuranosyl)-5-[1-(2,2,6,6-tetramethyl-1-ylooxypiperidin-4-yl)-1,2,3-triazol-4-yl]-7*H*-pyrrolo[2,3-*d*]pyrimidine (4): Compound **1** (137 mg, 0.5 mmol) and the 4-azido-2,2,6,6-tetramethylpiperidine 1-oxyl radical (**3**; 118 mg, 0.6 mmol) were dissolved in THF/H_2O/*t*BuOH (3:1:1, v/v, 5 mL) and then *N*,*N*-diisopropylethylamine (80 μL, 0.46 mmol) was added followed by the addition of copper(I) iodide (143 mg, 0.75 mmol). The reaction mixture was stirred for 4 h at room temperature. The solvent was evaporated and the residue was purified by FC (silica gel, column 4×10 cm, CH_2Cl_2/MeOH, 10:1) to give **4** as a pink solid, which was crystallized from H_2O to yield pink crystals (151 mg, 64%). R_f=0.53 (CH_2Cl_2/CH_3OH, 90:10); ^1H NMR (300 MHz, [D$_6$]DMSO, 25°C): δ=1.16–1.23 (m, 17H; 4 CH_3, 2 CH_2, CH, low intensity), 2.41 (br, 2H; 2′-H$_\alpha$, 2′-H$_\beta$), 3.48 (br, 2H; 5'-H), 3.84 (br, 1H; 4'-H), 4.38 (br, 1H; 3'-H), 5.04 (s, 1H; 5'-OH), 5.31 (s, 1H; 3'-OH), 6.57 (s, 1H; 1'-H), 7.39 (br, H; NH_2), 7.88 (s, 1H; 6-H), 8.10 (s, 1H; 2-H), 9.03 ppm (br, H; NH_2); UV/Vis (MeOH): λ_{max} (ε)=245 (14400), 279 nm (10800 $mol^{-1}m^3cm^{-1}$); MS (ESI): calcd for $C_{22}H_{31}N_8O_4$: 472.25; found: 472.25 $[M+H]^+$.

1-(2-Deoxy-β-D-*erythro*-pentofuranosyl)-5-[1-(2,2,6,6-tetramethyl-1-ylooxypiperidin-4-yl)-1,2,3-triazol-4-yl]uracil (5): As described for **4**, compound **2** (126 mg, 0.5 mmol) in THF/H_2O/*t*BuOH (3:1:1, v/v, 5 mL) was treated with the 4-azido-2,2,6,6-tetramethylpiperidine 1-oxyl radical (**3**) (118 mg, 0.6 mmol) in the presence of *N*,*N*-diisopropylethylamine (80 μL, 0.46 mmol) and copper(I) iodide (143 mg, 0.75 mmol). Purification by FC (silica gel, column 4×10 cm, CH_2Cl_2/MeOH, 10:1) gave **5** as a pink solid, which was crystallized from H_2O to yield light pink crystals (124 mg, 55%). R_f=0.46 (CH_2Cl_2/CH_3OH, 90:10); ^1H NMR (300 MHz, [D$_6$]DMSO, 25°C): δ=1.13–1.24 (m, 17H; 4 CH_3, 2 CH_2, CH, low intensity), 2.19 (br, 2H; 2′-H$_\alpha$, 2′-H$_\beta$), 3.59 (m, 2H; 5'-H), 3.85 (m, 1H; 4'-H), 4.28 (br, 1H; 3'-H), 5.03 (s, 1H; 5'-OH), 5.30 (s, 1H; 3'-OH), 6.24 (s, 1H; 1'-H), 8.59 (br, 1H; 6-H), 11.71 ppm (s, 1H; NH); UV/Vis (MeOH): λ_{max} (ε)=291 (14200), 232 nm (18400 $mol^{-1}m^3cm^{-1}$); MS (ESI): calcd for $C_{20}H_{29}N_6O_6$: 472.20; found: 472.20 $[M+Na]^+$.

General procedure for the cycloaddition of oligonucleotides with 4-azido-2,2,6,6-tetramethylpiperidine 1-oxyl (3): TBTA ligand (100 μL of a 20 mM stock solution in THF/H_2O/*t*BuOH, 3:1:1), *N*,*N*-diisopropylethylamine (2 μL of a 1% stock solution in water), CuI (10 μL, 20 mM stock solution in THF/H_2O/*t*BuOH, 3:1:1), and the 4-azido-2,2,6,6-tetramethylpiperidine 1-oxyl radical (**3**; 50 μL of a 20 mM stock solution in THF/H_2O/*t*BuOH, 3:1:1) were added to a ss-oligonucleotide (5 A_{260} units) and the reaction mixture was stirred at room temperature for 4 h. The reaction mixture was concentrated in a Speed-Vac, dissolved in bidistilled water (500 μL), and centrifuged for 30 min at 14000 rpm. The supernatant solution was collected and further purified by reversed-phase HPLC with the gradient 0–30 min 0–60% B in A, 30–40 min 60% B in A, 40–50 min 60–0% B in A, flow rate = 0.7 cm^3min^{-1}.

Acknowledgements

We thank Dr. S. Budow for continuous support throughout the preparation of the manuscript. We also thank S. S. Pujari for recording the NMR spectra, Dr. R. Thiele from Roche Diagnostics GmbH, Penzberg, Germany for the measurement of the MALDI-MS, and Nhat Quang Tran for oligonucleotide synthesis. Financial support by ChemBiotech, Münster, Germany (P.D.) and by the Volkswagenstiftung (I/79 950-952; D.W.) is gratefully acknowledged.

[1] a) W. Saenger, *Principles of Nucleic Acid Structure*, Springer-Verlag, New York, **1984**; b) V. A. Bloomfield, D. M. Crothers, I. Tinoco, Jr., *Nucleic Acids: Structures, Properties and Functions*, University Science Books, Sausalito, CA, **1999**, pp. 79–108.
[2] G. M. Blackburn, M. J. Gait, D. Loakes, D. M. Williams, *Nucleic acids in chemistry and biology, Vol. 5*, The Royal Society of Chemistry, Cambridge, **2006**, pp. 383–422.
[3] a) R. S. Keyes, A. M. Bobst in *Biological Magnetic Resonance: Spin labeling. The Next Millennium, Vol. 14* (Eds.: L. J. Berliner), Plenum Press, New York **1989**, pp. 283–334; b) O. Schiemann, T. F. Prisner, *Q. Rev. Biophys.* **2007**, *40*, 1–53; c) A. Marko, D. Margraf, P. Cekan, S. T. Sigurdsson, O. Schiemann, T. F. Prisner, *Phys. Rev. E* **2010**, *81*, 021911.
[4] G. Sicoli, G. Mathis, O. Delalande, Y. Boulard, D. Gasparutto, S. Gambarelli, *Angew. Chem.* **2008**, *120*, 747–749; *Angew. Chem. Int. Ed.* **2008**, *47*, 735–737.
[5] G. Sicoli, G. Mathis, S. Aci-Sèche, C. Saint-Pierre, Y. Boulard, D. Gasparutto, S. Gambarelli, *Nucleic Acids Res.* **2009**, *37*, 3165–3176.
[6] a) O. Schiemann, N. Piton, Y. Mu, G. Stock, J. W. Engels, T. F. Prisner, *J. Am. Chem. Soc.* **2004**, *126*, 5722–5729; b) O. Schiemann, A. Weber, T. E. Edwards, T. F. Prisner, S. T. Sigurdsson, *J. Am. Chem. Soc.* **2003**, *125*, 3434–3435.
[7] H.-J. Steinhoff, A. Savitsky, C. Wegener, M. Pfeiffer, M. Plato, K. Möbius, *Biochim. Biophys. Acta Bioenerg.* **2000**, *1457*, 253–262.
[8] H.-J. Steinhoff, *Biol. Chem.* **2004**, *385*, 913–920.
[9] P. P. Borbat, J. H. Freed, *Chem. Phys. Lett.* **1999**, *313*, 145–154.
[10] J. P. Klare, H.-J. Steinhoff, *Photosynth. Res.* **2009**, *102*, 377–390.
[11] a) A. Spaltenstein, B. H. Robinson, P. B. Hopkins, *Biochemistry* **1989**, *28*, 9484–9495; b) C. Giordano, F. Fratini, D. Attanasio, L. Cellai, *Synthesis* **2001**, 565–572.
[12] S. Obeid, M. Yulikov, G. Jeschke, A. Marx, *Angew. Chem.* **2008**, *120*, 6886–6890; *Angew. Chem. Int. Ed.* **2008**, *47*, 6782–6785.
[13] a) F. Hansske, K. Watanabe, F. Cramer, F. Seela, *Hoppe-Seyler's Z. Physiol. Chem.* **1978**, *359*, 1659–1665; b) P. Z. Qin, S. E. Butcher, J. Feigon, W. L. Hubbell, *Biochemistry* **2001**, *40*, 6929–6936; c) N.-K. Kim, A. Murali, V. J. DeRose, *Chem. Biol.* **2004**, *11*, 939–948; d) N. Piton, Y. Mu, G. Stock, T. F. Prisner, O. Schiemann, J. W. Engels, *Nucleic Acids Res.* **2007**, *35*, 3128–3143; e) Q. Cai, A. K. Kusnetzow, W. L. Hubbell, I. S. Haworth, G. P. Gacho, N. Van Eps, K. Hideg, E. J. Chambers, P. Z. Qin, *Nucleic Acids Res.* **2006**, *34*, 4722–4730.
[14] a) H. C. Kolb, M. G. Finn, K. B. Sharpless, *Angew. Chem.* **2001**, *113*, 2056–2075; *Angew. Chem. Int. Ed.* **2001**, *40*, 2004–2021; b) M. Meldal, C. W. Tornøe, *Chem. Rev.* **2008**, *108*, 2952–3015; c) F. Amblard, J. H. Cho, R. F. Schinazi, *Chem. Rev.* **2009**, *109*, 4207–4220; d) R. Huisgen, *Angew. Chem.* **1963**, *75*, 604–637; *Angew. Chem. Int. Ed. Engl.* **1963**, *2*, 565–598; e) R. Huisgen in *1,3-Dipolar Cycloaddition Chemistry, Vol. 2* (Eds: A. Padwa), Wiley, New York, **1984**; f) V. V. Rostovtsev, L. G. Green, V. V. Fokin, K. B. Sharpless, *Angew. Chem.* **2002**, *114*, 2708–2711; *Angew. Chem. Int. Ed.* **2002**, *41*, 2596–2599.
[15] P. M. E. Gramlich, C. T. Wirges, A. Manetto, T. Carell, *Angew. Chem.* **2008**, *120*, 8478–8487; *Angew. Chem. Int. Ed.* **2008**, *47*, 8350–8358.
[16] D. Graham, J. A. Parkinson, T. Brown, *J. Chem. Soc. Perkin Trans. 1* **1998**, 1131–1138.
[17] a) F. Seela, M. Zulauf, *Chem. Eur. J.* **1998**, *4*, 1781–1790; b) X. Peng, H. Li, F. Seela, *Nucleic Acids Res.* **2006**, *34*, 5987–6000; c) F. Seela, X. Peng, S. Budow, *Curr. Org. Chem.* **2007**, *11*, 427–462.
[18] F. Seela, V. R. Sirivolu, P. Chittepu, *Bioconjugate Chem.* **2008**, *19*, 211–224.
[19] F. Seela, M. Zulauf, *Synthesis* **1996**, 726–730.
[20] N. G. Bushmakina, A. Y. Misharin, *Synthesis* **1986**, 966–966.

[21] M. Kveder, G. Pifat, S. Pečar, M. Schara, P. Ramos, H. Esterbauer, *Chem. Phys. Lipids* **1997**, *85*, 1–12.
[22] a) P. Cekan, S. T. Sigurdsson, *J. Am. Chem. Soc.* **2009**, *131*, 18054–18056; b) M. Sajid, G. Jeschke, M. Wiebcke, A. Godt, *Chem. Eur. J.* **2009**, *15*, 12960–12962.
[23] N. D. Sinha, P. Davis, N. Usman, J. Pérez, R. Hodge, J. Kremsky, R. Casale, *Biochimie* **1993**, *75*, 13–23.
[24] M. Ahmadian, P. Zhang, D. Bergstrom, *Nucleic Acids Res.* **1998**, *26*, 3127–3135.
[25] D. Liang, L. Song, Z. Chen, B. Chu, *J. Chromatogr. A* **2001**, *931*, 163–173.
[26] S. Nagahara, A. Murakami, K. Makino, *Nucleosides Nucleotides* **1992**, *11*, 889–901.
[27] P. Z. Qin, K. Hideg, J. Feigon, W. L. Hubbell, *Biochemistry* **2003**, *42*, 6772–6783.
[28] M. Flaender, G. Sicoli, T. Fontecave, G. Mathis, C. Saint-Pierre, Y. Boulard, S. Gambarelli, D. Gasparutto, *Nucleic Acids Symp. Ser.* **2008**, *52*, 147–148.
[29] O. Schiemann, P. Cekan, D. Margraf, T. F. Prisner, S. T. Sigurdsson, *Angew. Chem.* **2009**, *121*, 3342–3345; *Angew. Chem. Int. Ed.* **2009**, *48*, 3292–3295.
[30] a) G. Jeschke, Y. Polyhach, *Phys. Chem. Chem. Phys.* **2007**, *9*, 1895–1910; b) J. E. Banham, C. M. Baker, S. Ceola, I. J. Day, G. H. Grant, E. J. J. Groenen, C. T. Rodgers, G. Jeschke, C. R. Timmel, *J. Magn. Reson.* **2008**, *191*, 202–218.
[31] C. Altenbach, W. L. Hubbell, *Biophys. J.* **2008**, *94*, *Supplement 1*, 826–832.
[32] H.-J. Steinhoff, N. Radzwill, W. Thevis, V. Lenz, D. Brandenburg, A. Antson, G. Dodson, A. Wollmer, *Biophys. J.* **1997**, *73*, 3287–3298.
[33] G. Jeschke, V. Chechik, P. Ionita, A. Godt, H. Zimmermann, J. Banham, C. R. Timmel, D. Hilger, H. Jung, *Appl. Magn. Reson.* **2006**, *30*, 473–489.
[34] a) E. Krieger, T. Darden, S. B. Nabuurs, A. Finkelstein, G. Vriend, *Proteins Struct. Funct. Bioinf.* **2004**, *57*, 678–683; b) E. Krieger, G. Koraimann, G. Vriend, *Proteins Struct. Funct. Bioinf.* **2002**, *47*, 393–402.
[35] V. Borsenberger, M. Kukwikila, S. Howorka, *Org. Biomol. Chem.* **2009**, *7*, 3826–3835.
[36] M. Pannier, S. Veit, A. Godt, G. Jeschke, H. W. Spiess, *J. Magn. Reson.* **2000**, *142*, 331–340.

Received: June 4, 2010
Published online: November 29, 2010

